ChemComm

Accepted Manuscript

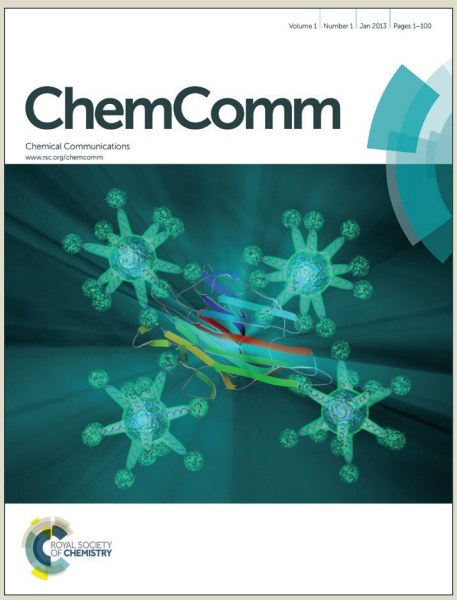

ROYAL SOCIETY OF CHEMISTRY

www.rsc.org/chemcomm

Journal Name

COMMUNICATION

Diverse Display of Non-covalent Interacting Elements using Pyrimidine-Embedded Polyheterocycles

Yoona Choi,[a,†] Heejun Kim,[a,†] Young-Hee Shin,[a] and Seung Bum Park*[,a,b]

Received 00th January 20xx,
Accepted 00th January 20xx

DOI: 10.1039/x0xx00000x

www.rsc.org/

A series of pyrimidine-embedded polyheterocycles was synthesized using pDOS strategy in a facile manner. The resulting poly-heterocyclic core skeletons containing unique aza-tricyclic framework allowed for diverse display of non-covalent interacting elements, which probably serve as essentials for perturbing specific non-covalent interactions between various biopolymers.

Phenotype-based screening is an inevitable choice for the discovery of novel bioactive chemical entities with new modes of action in the field of drug discovery and chemical biology, which can lead to the development of first-in-class therapeutics.[1–3] The collection of drug-like small molecules with high skeletal diversity plays a pivotal role in the discovery of promising small-molecule ligands using both a conventional target-based approach[4] and a phenotype-based approach.[5] For maximizing the molecular diversity in such a collection, the biomedical research community has applied diversity-oriented synthesis (DOS) as the major strategy.[6–8] Along with this endeavor, a privileged substructure-based DOS (pDOS) strategy has emerged for the generation of the novel collection of drug-like small molecules exhibiting high efficiency and improved biological relevance.[9] In addition, this pDOS strategy focuses on the reconstruction of diverse and unprecedented drug-like polyheterocycles, which are embedded with privileged substructures frequently observed in bioactive natural products and therapeutic agents.[10] The unique value of a pDOS library has been demonstrated by the identification of novel small-molecule modulators exhibiting various therapeutic effects toward neuroinflammation,[11] type II diabetes,[12] stem-cell differentiation,[13] and cancer.[14]

For maximizing the coverage of chemical space employing pDOS strategy, we focused on the diversification of conformationally restricted polyheterocycles in a three-dimensional (3-D) space.[15,16] Meanwhile, we also envisioned that the small-molecule-based perturbation of specific biopolymers can be achieved by a unique display of diverse non-covalent interacting elements, especially electrostatic and hydrogen-bonding interactions, within a well-defined single molecular framework containing privileged substructures.

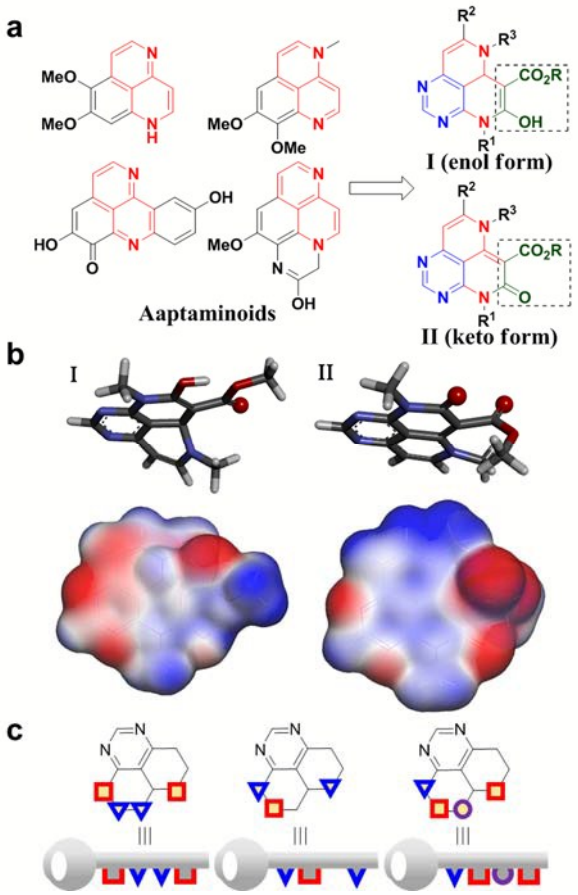

Fig. 1 (a) Chemical structures of marine alkaloid—aaptaminoids and pyrimidine-containing polyheterocyclic skeletons **I** and **II**; (b) Energy-minimized conformers of the two skeletons and their polar surface area illustrated by the isosurface diagrams; (c) Unique display of non-covalent interacting elements within pyrimidine-containing polyheterocycles.

[a.] *Department of Chemistry, Seoul National University, Seoul 151-747, Korea.*
[b.] *WCU Department of Biophysics and Chemical Biology/N-Bio institute, Seoul National University, Seoul 151-747 Korea.*
† These authors contributed equally.
Electronic Supplementary Information (ESI) available: Additional figures, full characterization and spectroscopic data of all new compounds, and detailed experimental protocols. See DOI: 10.1039/x0xx00000x

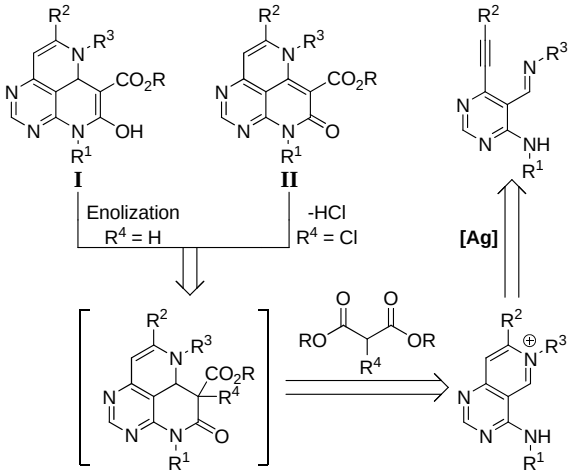

Fig. 2 Retrosynthetic analysis of skeleton **I** and **II**

For this purpose, we explored various skeletons that can uniquely display diverse non-covalent interacting elements using single polyheterocycles with high biological relevance. Among those attempts, we designed pyrimidine-embedded aza-tricyclic skeletons containing a structural framework similar to that of aaptaminoids,[17] which are natural marine alkaloids exhibiting various bioactivities such as anticancer,[18] antiviral,[19] and antifungal activities (Fig. 1a).[20] These skeletons **I** and **II** not only employed unique skeletal features of aaptaminoids, but also exhibited distinguishable polar surface area and hydrogen-bonding capability, caused by the differentiation of the enol and keto forms, respectively (Fig. 1b). In addition, the existence of one sp^3 carbon in skeleton **I** allowed for the 3-D discrete conformation different from that of skeleton **II**. Moreover, skeletons **I** and **II** were designed to accommodate diverse non-covalent interacting elements, such as electrostatic interactions, hydrogen bonding, and even hydrogen atom, within a single polyheterocyclic skeleton (Fig. 1c).

For preparing the skeletons **I** and **II**, a cascade cyclization strategy was adopted starting from tri-substituted *ortho* alkynylpyrimidine aldimine. As shown in Fig. 2, the key substrate aldimines were first transformed into bicyclic pyridinium intermediates by Ag-catalyzed 6-*endo* cyclization.[21] Next, the resulting pyridinium compounds were subjected to nucleophilic addition with dialkyl malonates,[22] followed by cyclization via simultaneous lactamization with the amino group at the 4 position of the pyrimidine ring. After the formation of the tricyclic core structures, skeletons **I** and **II** were differentiated by enolization (in the case of R^4 = H) and dehydrodechlorination (in the case of R^4 = Cl), respectively. This unique three-step transformation allows for the efficient one-pot preparation of skeletons **I** and **II**.

To construct the molecular collection of skeletons **I** and **II**, the facile condensation[22] between aldehydes (**4–9**) and various amines afforded stable imines **4a'–9f'** (Table 1, Step 1). The molecular diversity of skeletons **I** and **II** was readily achieved by the combination of various R^1, R^2, and R^3 groups, such as aliphatic, aromatic, heterocyclic, and/or carbocyclic motifs, affording products in high yields (average 83%, Table 1). In Step 2, the tandem cyclization of the imines prepared in Step 1 with dimethyl malonate provided pyrimidine-containing tricyclic cores, which were spontaneously tautomerized to the enol form (skeleton **I**), caused by the conjugation effect and the intramolecular hydrogen bonding with the malonate-derived ester group. This tandem cyclization protocol afforded a series of polyheterocycles containing skeleton **I** in an average yield of 70%, irrespective of the R^1, R^2, and R^3 substituents. For skeleton **II**, the nucleophilic addition of diethyl chloromalonate, instead of dimethyl malonate, to the iminium intermediates afforded the keto form (skeleton **II**) by lactamization and the subsequent removal of hydrochloride (Table 2). This tandem three-step cyclization provided a series of polyheterocycles containing skeleton **II** in moderate-to-good yields. Hence, such a divergent strategy at the later stage of synthesis efficiently afforded two unique skeletons containing different non-covalent interacting elements.

Table 1 Synthesis of imines as well as the collection of polyheterocycles containing skeleton **I**[a]

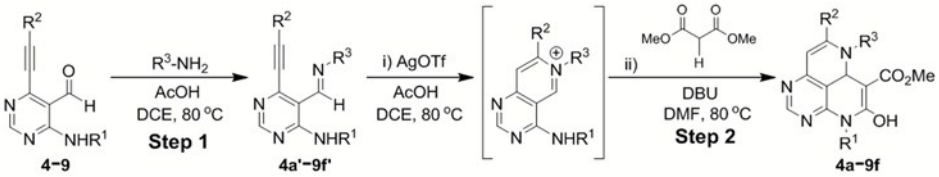

R1	R2 \ R3		a	b	c	d	e	f
CH3		4	86[b] / 95[c]	84 / 70	89 / 76	91 / 69	91 / 62	86 / 78
		5	66 / 77	68 / 83	74 / 79	80 / 58	84 / 69	95 / 49
		6	83 / 74	66 / 87	99 / 76	93 / 53	93 / 87	95 / 47
		7	67 / 61	62 / 70	84 / 91	88 / 70	85 / 67	86 / 56
		8	66 / 62	69 / 85	94 / 74	83 / 48	84 / 64	92 / 48
		9	87 / 67	61 / 92	95 / 72	92 / 65	71 / 64	92 / 55

[a] See ESI for detailed experimental procedures; [b] Isolated yields of Step 1; [c] Isolated yields of Step 2.

Table 2 Synthesis of the collection of polyheterocycles containing skeleton **II**[a]

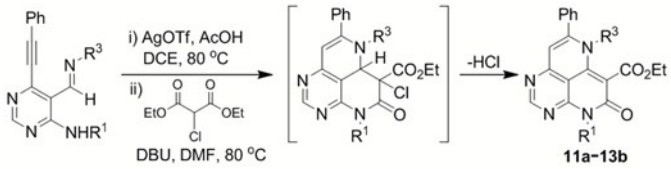

Product	R^1	R^3	Yield(%)[b]
11a	methyl	2-methoxyethyl	53
11b		4-methoxyphenyl	76
11c		benzyl	69
11d		3,4-dimethxoyphenethyl	57
11f		1-Boc-4-(aminomethyl)piperidyl	53
11g		4-methoxybenzyl	60
12a	benzyl	2-methoxyethyl	52[c]
12b		4-methoxyphenyl	53
12c		benzyl	53[c]
12d		3,4-dimethoxyphenethyl	52
13a	4-methoxybenzyl	2-methoxyethyl	48[c]
13b		4-methoxyphenyl	57

[a]See ESI for detailed experimental procedures. [b]Isolated yields. [c]*t*-BuOH was used as solvent instead of DMF.

For the discrete display of various non-covalent interacting elements in a single polyheterocyclic framework, we further diversified the representative compounds from skeleton **I** and **II**. As shown in Fig. 3, we analyzed each substituent using different color codes to reveal the different capability of non-covalent interactions, such as H-bonding donor, H-bonding acceptor, as well as electrostatic interactions and hydrogen atom. For example, a code of A-D-A-A for compound **4a** suggests that it consists of a H-bonding acceptor, a H-bonding donor, a H-bonding acceptor, and a H-bonding acceptor at the color-coded sites by the sequence of the curved arrow (Fig. 3). This code differentiates the resulting collection of each polyheterocycle containing unique arrays of non-covalent interacting elements. Accordingly, ten differently coded structures were generated from the single molecular framework, which can induce specific interactions with various biopolymers.

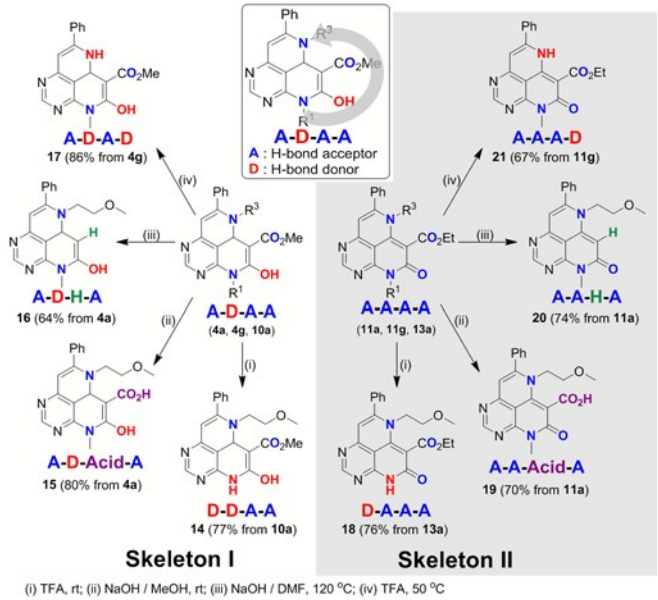

Fig. 3 Distinct display of diverse non-covalent interacting elements on pyrimidine-embedded polyheterocycles

For visualizing the molecular diversity of differently coded structures, especially their electrostatic polar surface area, energy minimized conformers as well as the isosurface diagrams of each representative compound with different codes were obtained by the calculation of electrostatic potentials and electron density. As shown in Fig. 4, a molecular set having different codes exhibited discrete distributions for the polar surface area in a single molecular framework. This result indicates that by using a well-defined aza-tricyclic molecular framework, which demonstrates potential for inducing discrete biological events, the pyrimidine-containing polyheterocyclic skeletons **I** and **II** can display diverse non-covalent interacting elements.

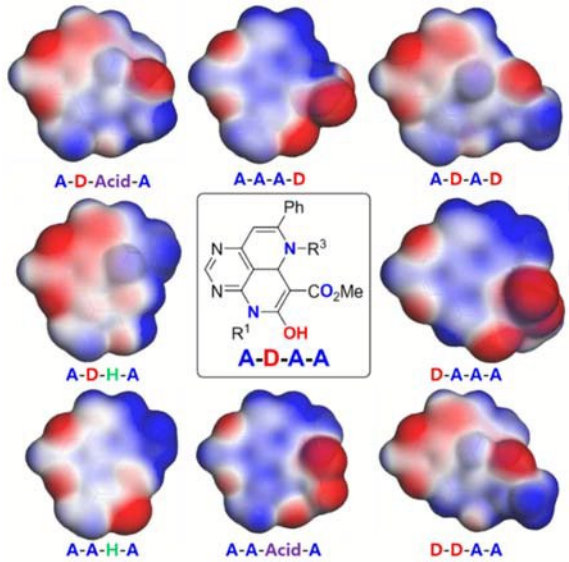

Fig. 4 Polar surface areas of eight differently coded structures are illustrated by isosurface diagram (isovalue is set as 0.017C).

After constructing a series of aza-tricycles containing skeletons **I** and **II**, we hypothesized that this pDOS strategy probably results in different biological activities on the basis of their display patterns of non-covalent interacting elements. Hence, to test this hypothesis, we made a collection of pyrimidine-embedded polyheterocycles with 10 different codes (Fig. 3) and subjected them to cell viability assays and several image-based phenotypic screenings. Among these screening experiments, the results from the high-content screening for autophagy or cellular lipid biogenesis[23] by monitoring a lipid droplet (LD) with the use of a fluorogenic bioprobe SF44[24] exhibited an interesting pattern. As shown in Figs. 5a and 5b, the changes of cellular LDs in human cervical cancer HeLa cells can be easily quantified by the fluorescence intensity of SF44. Surprisingly, the cellular LDs in HeLa cells were decreased upon treatment with compounds containing skeleton **I**, whereas those in HeLa cells were not decreased by compounds containing skeleton **II** (Fig. 5c). Among the derivatives containing skeleton **I**, **16** exhibited the best potency for LD decrease in a dose-dependent manner without cellular cytotoxicity; however, its ketone counterpart **20** did not affect the cellular LDs (Figs. 5a, 5d, and S4, ESI†). Previously, we have reported that the changes in the LDs can be induced by the perturbation on lipid biogenesis or an autophagy-related recycling pathway.[23] To test whether **16** affects cellular LD levels by autophagy, we performed western blot analysis for monitoring the changes in the autophagy

biomarkers microtubule-associated protein 1 light chain 3 (LC3) and p62; the conversion of LC3 I to LC3 II was related to the maturation of autophagosome, and the degradation of p62 reflects the entire flux of the autophagic process. As shown in Fig 5e, the treatment with **16** did not affect the change of the p62 level as well as the conversion ratio of LC3 I to II, indicating that **16** does not reduce cellular LDs by the activation of autophagy. Even though the mechanistic study on the inhibition of lipid biogenesis is currently underway, this drastic difference in the phenotypic changes is quite interesting, especially in the lipid biogenesis, by simple changes between the enol and keto forms in pyrimidine-embedded polyheterocycles.

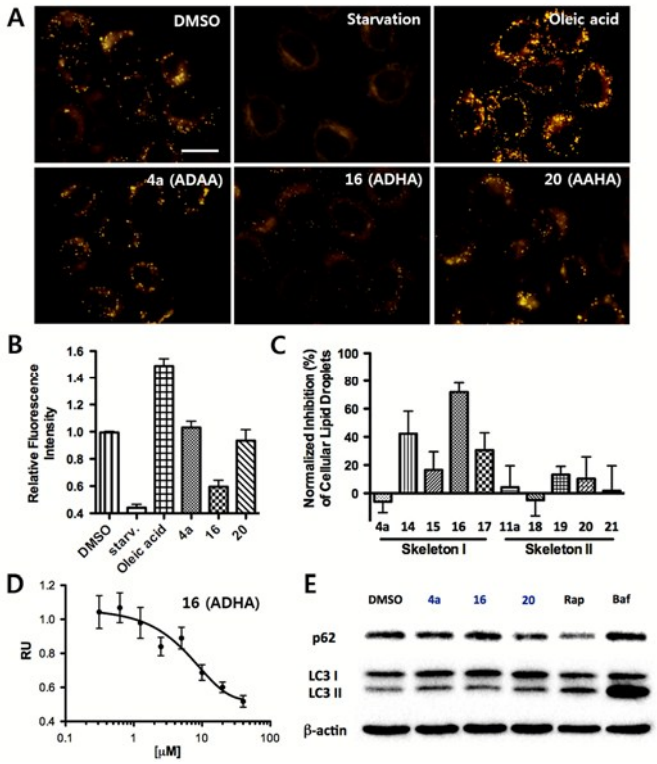

Fig. 5 Cell-based phenotypic analysis for the evaluation of the different bioactivities exhibited by the representative coded compounds. (a) Fluorescence micrographs showing cellular LDs in HeLa cells stained with SF44. Cells were incubated with DMSO, serum-free media, oleic acid (5 μM), **4a**, **16**, and **20** (10 μM). Scale bar: 20 μm; (b) Quantified fluorescence intensities of cellular LDs represented in Fig. 5a; (c) Normalized cellular LD inhibition (%) exhibited by 10 coded compounds shown in Fig. 3; (d) A dose-response curve of cellular LDs in relative unit (RU) upon treatment with **16**; (e) Western blot data monitoring the conversion of microtubule-associated protein 1 light chain 3 (LC3) I to LC3 II and the degradation of p62 upon treatment with DMSO, **4a**, **16**, **20** (10 μM each), rapamycin (Rap, 200 nM), and bafilomycin (Baf, 100 nM).

In conclusion, we successfully constructed pyrimidine-based polyheterocycles containing the aza-tricyclic core skeletons, which share the structural features of bioactive marine alkaloids —aaptaminoids. For diverse display of non-covalent interacting elements using this unique polyheterocyclic framework, we designed and synthesized two distinct skeletons; skeletons **I** and **II** were differentiated by the enol and keto forms, which exhibit different H-bonding abilities and polar surface areas. The further diversification of substituents afforded 10 different coded structures with discrete non-covalent interacting elements as well as the different distribution of polar surface areas. The utility of this pyrimidine-based pDOS pathway was confirmed by the differential bioactivities of skeletons **I** and **II** using image-based high-content screening for lipid biogenesis and autophagy.

Notes and references

This work was supported by the National Creative Research Initiative Grant (2014R1A3A2030423) and Bio & Medical Technology Development Program (2012M3A9C4048780) through the National Research Foundation of Korea (NRF) funded by the Korean Government (Ministry of Science, ICT & Future Planning). Y.C. and H.K. are grateful for their predoctoral fellowship awarded by the BK21 Plus Program.

1 D. C. Swinney, *Clin. Pharmacol. Ther.*, 2013, **93**, 299.
2 D. C. Swinney, and J. Anthony, *Nat. Rev. Drug Discovery*, 2011, **10**, 507.
3 S. L. Schreiber, *Nature*, 2009, **457**, 153.
4 C. Lipinski, A. Hopkins, *Nature*, 2004, **432**, 855.
5 W.R.J.D Galloway, and D. R. Spring, *Expert Opin. Drug Discovery*, 2009, **4**, 467.
6 D. S. Tan, *Nat. Chem. Biol.*, 2005, **1**, 74.
7 W. R. J. D. Galloway, A. Isidro-Llobet, and D. R. Spring, *Nat. Commun.*, 2010, **1**, 80.
8 C. J. O'Connor, H. S. G. Beckmann, and D. R. Spring, *Chem. Soc. Rev.*, 2012, **41**, 4444.
9 S.-M Oh, and S. B. Park, *Chem. Commun.*, 2011, **47**, 12754..
10 J. Kim, H. Kim, and S. B. Park, *J. Am. Chem. Soc.*, 2014, **136**, 14629.
11 S. Lee, Y. Nam, J. Y. Koo, D. Lim, J. Park, J. Ock, K. Suk, and S. B. Park, *Nat. Chem. Biol*, 2014, **10**, 1055.
12 Oh, S. J. Kim, J. H. Hwang, H. Y. Lee, M. J. Ryu, J. Park, S. J. Kim, Y. S. Jo, Y. K. Kim, C. H. Lee, K. R. Kweon, M. Shong, and S. B. Park, *J. Med. Chem.*, 2010, **53**, 7405.
13 J. Kim, T.–J, Cho, S.-K. Kwon, K. Oh, J.-a Lee, D.-S. Lee, J. Cho and S. B. Park, *Chem. Sci.*, 2012, **3**, 3071.
14 J. Park, S. Oh, and S. B. Park, *Angew. Chem. Int. Ed.*, 2012, **51**, 5447.
15 S. K. Ko, H. J. Jang, E. Kim, and S. B. Park, *Chem. Commun.*, 2006, **28**, 2962.
16 H. Kim, T. T. Tung, and S. B. Park, *Org. Lett.*, 2013, **15**, 5814.
17 E. L. Larghi, M. L. Bohn, and T. S. Kaufman, *Tetrahedron*, 2009, **65**, 4257.
18 Y.-C. Shen, T.-T. Lin, J.-H. Sheu, and C.-Y. Duh, *J. Nat. Prod.*, 1999, **62**, 1264.
19 T. M. L. Souza, J. L. Abrantes, R. A. Epifanio, C. F. L. Fontes, and I. C. P. Fruguhetti, *Planta Med.*, 2007, **73**, 200.
20 B. Fugmann, B. Steffan, and W. Steglich, *Tetrahedron Lett.*, 1984, **25**, 3575.
21 A. Naoki, Y. S. Salprima, N. Tsutomu, and Y. Yoshinori, *Angew. Chem. Int. Ed.*, 2005, **44**, 5526.
22 C. Inga, B. Rita, R. Simonas, M. Marius, and M. Dainius, *Tetrahedron*, 2010, **66**, 251.
23 S. Lee, E. Kim, and S. B. Park, *Chem. Sci.*, 2013, **4**, 3282.
24 E. Kim, S. Lee, and S. B. Park, *Chem. Commun.*, 2012, **48**, 233.